

Catalytic Hydrothermal Liquefaction of Water Hyacinth Using Fe₃O₄/NiO Nanocomposite: Optimization of Reaction Conditions by Response Surface Methodology

Godwin Aturagaba, Dan Egesa*, Edward Mubiru, Emmanuel Tebandeke

Department of Chemistry, College of Natural Sciences, School of Physical Sciences, Makerere University, Kampala, Uganda

Email: *dan.egesa@mak.ac.ug, *daniegesa4@gmail.com

How to cite this paper: Aturagaba, G., Egesa, D., Mubiru, E. and Tebandeke, E. (2023) Catalytic Hydrothermal Liquefaction of Water Hyacinth Using Fe₃O₄/NiO Nanocomposite: Optimization of Reaction Conditions by Response Surface Methodology. *Journal of Sustainable Bioenergy Systems*, 13, 73-98.

<https://doi.org/10.4236/jsbs.2023.133005>

Received: June 12, 2023

Accepted: July 28, 2023

Published: July 31, 2023

Copyright © 2023 by author(s) and Scientific Research Publishing Inc. This work is licensed under the Creative Commons Attribution International License (CC BY 4.0).

<http://creativecommons.org/licenses/by/4.0/>



Open Access

Abstract

This research aimed at optimizing the reaction conditions for the catalytic hydrothermal liquefaction (HTL) of water hyacinth using iron oxide/nickel oxide nanocomposite as catalysts. The iron oxide/nickel oxide nanocomposite was synthesized by the co-precipitation method and used in the hydrothermal liquefaction of water hyacinth. The composition and structural morphology of the synthesized catalysts were determined using X-ray diffraction (XRD), transmission electron microscopy (TEM), scanning electron microscopy (SEM), and atomic absorption spectroscopy (AAS). The particle size distribution of the catalyst nanoparticles was determined by the Image J software. Three reaction parameters were optimized using the response surface methodology (RSM). These were: temperature, residence time, and catalyst dosage. A maximum bio-oil yield of 59.4 wt% was obtained using iron oxide/nickel oxide nanocomposite compared to 50.7 wt% obtained in absence of the catalyst. The maximum bio-oil yield was obtained at a temperature of 320°C, 1.5 g of catalyst dosage, and 60 min of residence time. The composition of bio-oil was analyzed using gas chromatography-mass spectroscopy (GC-MS) and elemental analysis. The GC-MS results showed an increase of hydrocarbons from 58.3% for uncatalyzed hydrothermal liquefaction to 88.66% using iron oxide/nickel oxide nanocomposite. Elemental analysis results revealed an increase in the hydrogen and carbon content and a reduction in the Nitrogen, Oxygen, and Sulphur content of the bio-oil during catalytic HTL compared to HTL in absence of catalyst nanoparticles. The high heating value increased from 33.5 MJ/Kg for uncatalyzed hydrothermal liquefaction to 38.6 MJ/Kg during the catalytic HTL. The catalyst nanoparticles were recovered from the solid residue by sonication and magnetic separation and recycled. The re-

cycled catalyst nanoparticles were still efficient as hydrothermal liquefaction (HTL) catalysts and were recycled four times. The application of iron oxide/nickel oxide nanocomposites in the HTL of water hyacinth increases the yield of bio-oil and improves its quality by reducing hetero atoms thus increasing its energy performance as fuel. Iron oxide/nickel oxide nanocomposites used in this study are widely available and can be easily recovered magnetically and recycled. This will potentially lead to an economical, environmentally friendly, and sustainable way of converting biomass into biofuel.

Keywords

Catalytic Hydrothermal Liquefaction, Water Hyacinth, Bio-Oil, Central Composite Design, Response Surface Methodology, Optimization

1. Introduction

Carbonaceous fuel is the major energy source used in daily activities such as cooking, transportation, and industrial processes [1]. Currently, fuels can be categorized into fossil fuels and biofuels depending on the source. Fossil fuel-based energy which is our primary source of energy is non-renewable and can emit harmful air pollutants when burnt. For many decades, the increasing world population has relied on these fossil fuels for the production of transportation, industrial and household fuels, and petrochemicals [2]. There has been a reduction in conventional crude oil production since 2004 when it was at its peak at 74 million barrels per day, and the combusted fossil fuels continuously release trapped carbon into the atmosphere in the form of carbon dioxide (CO₂), a greenhouse gas [3]. Therefore, the depletion of fossil fuels is certain.

These challenges have motivated research into alternative clean, renewable, and sustainable sources of energy such as solar energy, geothermal power, wind energy, and biofuels. Biofuels are being considered as a suitable alternative energy source due to the abundance of renewable energy resources which are carbon neutral. Biofuels are broadly defined as solid, gaseous, or liquid fuels produced from bio-renewable resources derived from biomass [4]. Biofuels can be classified into three generations depending on the sources of biomass [1]. These are the first-generation, second-generation, and third-generation. First-generation biofuels are produced primarily from edible biomass like sugarcane and soybean [5]. Second-generation biofuels are produced from a large variety of feedstock ranging from lignocellulosic feedstock materials to municipal solid wastes, and third-generation biofuels are derived from aquatic biomass [6] [7]. The biomass used to produce second and third-generation biofuels is preferred to the edible biomass used to produce first-generation biofuel to avoid fuel versus food competition. Water hyacinth (*Eichhornia crassipes*) is a promising biofuel source because of its potential to produce huge quantities of biomass and can be cultivated on large water bodies thus eliminating the competition for fertile agricultural land.

Water hyacinth is a carbon-rich renewable energy source and its biomass is made of 18% - 31% cellulose, 18% - 42% hemicellulose, and 7% - 26% lignin which favors biofuel production [8] [9] [10]. Regardless of its great potential for biomass production, water hyacinth is considered a nuisance weed and discarded as waste [8]. This is because the invasion of water hyacinths on freshwater bodies disrupts water transport and hydropower generation, reduces fish catch, and pollutes freshwater. Therefore, the conversion of this unexploited wet biomass into biofuel would be a positive development in this energy crisis era.

Biomass can be converted to biofuels (solid, liquid, and gas fuels) through either biochemical or thermochemical technologies but the latter is widely used because it is fast [11] [12]. Among the thermochemical conversion technologies (carbonization, gasification, hydrothermal liquefaction, pyrolysis, and combustion), only pyrolysis and hydrothermal liquefaction can ably produce liquid fuel directly from solid biomass [13]. The hydrothermal liquefaction (HTL) process is preferred in the conversion of water hyacinth biomass into bio-oil due to its capability to convert wet biomass thus eliminating the need for drying biomass which makes the process energy efficient. During hydrothermal liquefaction, the biomass in presence of water at a medium temperature (250°C - 400°C) and high pressure (40 - 220 bar) is decomposed to a solid phase, liquid phase, and a gas phase mainly constituted by carbon dioxide [14]. The bio-oil is largely extracted from the solid residue phase.

The bio-oil obtained from the hydrothermal liquefaction process of lignocellulosic biomass presents yields of about 20% - 40% and still contains large quantities of oxygen (20% - 30%) [11] [14] leading to a reduction in higher heating value, high acidity, instability, and immiscibility. Significant effort has been made to improve the quality and quantity of biofuels. A promising approach is the use of catalysts in the hydrothermal liquefaction process. The bio-oil compounds can be significantly influenced by catalysts during the hydrothermal liquefaction process thus increasing the quality of biofuel.

Catalysts in the hydrothermal liquefaction process offer several advantages which include increasing the bio-oil yield and biomass conversion, boosting the flow properties of biofuel, lowering the biofuel heteroatom content, and reducing the temperature required for achieving the higher biofuel yield [15]. Catalysts used in the hydrothermal liquefaction process may be homogeneous or heterogeneous. Homogeneous catalysis by acids, alkali, or metal salts has been used in the hydrothermal liquefaction process because they are cheap but their corrosiveness and difficulties in recovery have reduced their application directing attention to the heterogeneous catalysts [16]. These catalysts also offer easy recovery, low corrosion rate, and high catalytic activity compared to homogeneous catalysts [17]. Several homogeneous and heterogeneous catalysts used in improving the bio-oil yield in the hydrothermal liquefaction process have been reviewed suggesting that the heterogeneous catalyst has a higher conversion efficiency than homogeneous catalysts [2].

When a heterogeneous catalyst (Fe) was used in the hydrothermal liquefaction of water hyacinth, the bio-oil yield increased from 16 wt% to 30.39% compared to K_2CO_3 (bio-oil yield: 22%) and KOH (bio-oil yield: 23%). This was obtained at similar operating conditions of temperature (280°C), residence time (15 minutes), and the biomass-to-water ratio of 1:6 revealing that heterogeneous catalysts were more efficient than homogeneous catalysts during hydrothermal liquefaction [18] [19].

Iron oxide nanocatalysts have great potential in the hydrothermal liquefaction process because they exhibit high catalytic activity, have a high specific surface area, have less resistance to mass transfer, are economically friendly, and can be separated by a magnetic field and reused [20]. In our recent study on the effect of process conditions and magnetite nanoparticles on bio-crude yield and composition during the hydrothermal liquefaction of water hyacinth, the highest bio-oil yield was 58.3 wt% compared to 52.3 wt% in absence of magnetic nanoparticles at a temperature of 320°C, a residence time of 60 minutes, magnetic nanoparticles to biomass ratio of 0.2 g/g, and biomass to water ratio of 0.06 g/g. The characterization of the bio-oil composition suggested the Fe_3O_4 nanocatalyst improved the yield and quality of the bio-oil. Modification of iron oxide nanocatalysts with other transition metal oxides may improve the quality and yield of biofuels produced by the hydrothermal liquefaction process. This is because some transition metal oxides like nickel oxide demonstrated great deoxygenating ability in previous studies [21], and combining them with iron oxide potentially creates favorable synergistic effects.

This research investigated the effect of Fe_3O_4/NiO nanocomposite catalysts on the yield and quality of bio-oils in the HTL of water hyacinth and optimized the reaction conditions using response surface methodology.

2. Materials and Methods

2.1. Materials

Iron (II) sulphate heptahydrate (ferrous sulphate), iron (III) sulphate hydrate (ferric sulphate), nickel sulphate hexahydrate, sodium hydroxide, ammonium hydroxide, hydrochloric acid, ethanol, dichloromethane were purchased from Laboratory needs solutions in Kampala, Uganda. The stalk and leaf of water hyacinth were collected from the shores of Lake Victoria in Gaba, Uganda 0°15'53" North, 32°37'38" East. All chemicals and reagents used were of analytical grade and the typical composition of the water hyacinth biomass is as follows: cellulose (18% - 31%), hemicellulose (18% - 43%), lignin (7% - 26%), protein (average of 7.11%) and fat (average of 1.9%) among other constituents [8] [9].

2.2. Methods

2.2.1. Synthesis of Catalyst Nanoparticles

1) Synthesis of iron oxide nanocatalyst

Following a previously reported procedure [20], the iron oxide nanocatalyst

was synthesized by a one-step co-precipitation method without any stabilizing agent. Briefly, hydrated iron (III) sulphate, $\text{Fe}_2(\text{SO}_4)_3 \cdot x\text{H}_2\text{O}$ (8.0 g) and hydrated iron (II) sulphate, $\text{FeSO}_4 \cdot 7\text{H}_2\text{O}$ (2.8 g) were dissolved in hydrochloric acid (0.2 mol/L, 25 cm³). Ammonium hydroxide solution (1.5 mol/L, 200 cm³) was added dropwise to the resultant solution with vigorous stirring at 300 rpm for 2 hr. A black precipitate formed and was decanted from the solvent magnetically. The catalyst was then washed with de-oxygenated distilled water and ethanol. The catalyst was dried at 70 °C in a hot air oven for 2 hr and stored in a desiccator.

2) Synthesis of iron oxide/nickel oxide nanocomposite

Following the previously reported procedure [22], hydrated nickel (II) sulphate, $\text{NiSO}_4 \cdot 6\text{H}_2\text{O}$ (2.70 g), and sodium hydroxide, NaOH (0.8 g) were put in two separate beakers. Then the content of each beaker was dissolved in distilled water (20 mL). Iron oxide nanoparticles, Fe_3O_4 (0.2 g) were added to the beaker containing nickel (II) ions. Sodium hydroxide solution was then added dropwise to the solution containing nickel ions and iron oxide nanoparticles with vigorous stirring at 300 rpm using a mechanical stirrer for 90 minutes. The resulting product was filtered and washed several times using distilled water. The product obtained was dried in the oven for 2 hr at 70 °C. It was then calcined at 300 °C for 2 hr.

2.2.2. Biomass Preparation

The water hyacinth leaves and stalk were washed with tap water to remove dirt. It was then cut into smaller pieces. The chopped pieces were oven-dried at 60 °C, milled to powder, and passed through a mesh sieve. The powder samples were placed into plastic bags, sealed, and stored in a dry place for further experimental use. The moisture and ash content in the biomass powder was determined gravimetrically as in our previous study [5].

2.2.3. Hydrothermal Liquefaction of Water Hyacinth Biomass

HTL experiments were carried out in a 100 ml stainless steel batch reactor autoclave (CF series) fitted with a pressure gauge and a thermocouple to record the temperature. The HTL experiments were performed at different reaction conditions of residence time, catalyst dosage, and temperature. A specified mass of the catalyst was thoroughly mixed with water hyacinth (5 g) and loaded into the reactor. Distilled water (90 g) was added to the mixture in the reactor to form a paste and tightly sealed. A specified temperature was set and the reactor transferred to the heating mantle. The reaction was allowed to stand for the specified time. After the reaction, the reactor was cooled with running tap water. The product gas was vented off while the liquid-solid products were filtered using a Whatman filter paper. The aqueous phase was dried in the oven at 50 °C to obtain water-soluble products and the residue was dissolved in dichloromethane (DCM). This mixture was filtered to obtain the DCM phase as the filtrate containing the heavy bio-oil (HO) and the solid residue was oven-dried. The bio-oil in the aqueous phase was dissolved in DCM. After evaporating the DCM phase,

the bio-oil yield in the aqueous phase (light oil) was added to the bio-oil yield in the solid phase (heavy oil) to get the total bio-oil yield.

The bio-oil was also recovered using a rotary evaporator (BUCHI R-300) operated under vacuum at 40°C and a rotation speed of 30 rpm to remove DCM.

Figure 1 illustrates the separation procedure.

Equation (1) was used to determine the percentage bio-oil yield.

$$Y_{BO} = \frac{W_{BO}}{W_{WH} - (W_A + W_M)} \times 100\% \quad (1)$$

Where Y_{BO} is the percentage yield of bio-oil, W_{BO} is the mass of bio-oil, W_{WH} is the mass of water hyacinth powder, W_A is the mass of ash content, and W_M is the mass of moisture content.

Equation (2) was used to determine the energy recovery.

$$ER = \frac{HHV_{BO} \times W_{BO}}{HHV_{WH} \times W_{WH}} \times 100\% \quad (2)$$

where ER is the energy recovery, HHV_{BO} is the high heating value of bio-oil, W_{BO} is the mass of bio-oil, HHV_{WH} is the high heating value of water hyacinth, and W_{WH} is the mass of water hyacinth feedstock.

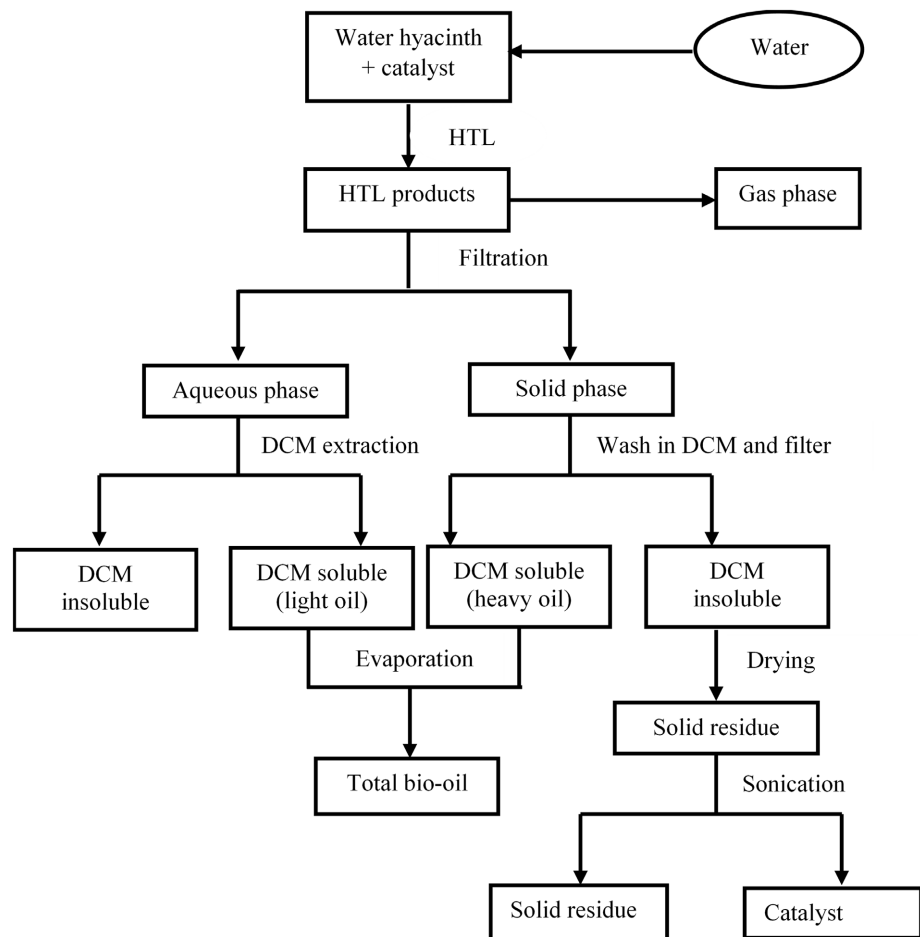


Figure 1. Illustration of the separation procedure.

The process conditions were fixed by the central composite design of the response surface methodology. The factors were set as follows; temperature (260°C to 320°C), residence time (15 minutes to 60 minutes), and catalyst concentration (0.25 g to 1.5 g). The response surface methodology tool provided 20 runs with different operating conditions. Furthermore, Equation (1) was used to calculate bio-oil yield, and Equation (2) was used to calculate energy recovery. The response surface methodology tool was used to plot the contour plots and response surface 3D graphs. Bio-oil samples were analyzed for elemental composition using a Thermo model EA1110 elemental analyzer, running Xperience EA software, single tube configured for oxygen analysis using a Molecular Sieve 3A separation column. References and samples were weighed to 6 decimal places using a Mettler UMX5 microbalance. Equation (3) is the Dulong formula used to determine the HHV of the bio-oil produced [23].

$$\text{HHV}(\text{MJ} \cdot \text{kg}^{-1}) = 0.3383C + 1.428\left(\text{H} - \frac{\text{O}}{8}\right) + 0.095S \quad (3)$$

where C, H, O, and S are the weight percentages of carbon, hydrogen, oxygen, and Sulphur respectively.

2.2.4. Recycling of Catalyst Nanoparticles

The catalyst nanoparticles were recovered following the method of Egesa *et al.* [20]. In this method, the dry solid residue containing catalyst nanoparticles was suspended in de-ionized and deoxygenated water and sonicated for 10 to 30 minutes. The biomass floated to the surface of the water from where it was skimmed off and the catalyst recovered magnetically. This recovery/cleaning process was repeated at least twice to recover a clean and biomass-free catalyst. The recovered catalyst was then weighed and recycled for further HTL reactions under similar reaction conditions.

2.2.5. Analytical Techniques

The iron oxide nanocatalyst was characterized in the same way as in our previous study [5]. Briefly, the Shape, size, and dispersion of the MNPs were analyzed using a JEM-1200 EX11 transmission electron microscope (TEM) at an acceleration voltage of 300 Kv. The size distribution of the nanocatalyst was determined using Image J software. The crystal structure and phase composition of nanocatalyst were characterized on a Bruker D8 Advanced X-ray diffraction (XRD) machine operating at 40 kV and 80 mA and a scanning rate of 0.02°/s in 2θ range from 20° to 70° and wavelength of 1.54056 Å. Iron oxide/nickel oxide nanocomposite was characterized using Flame atomic absorption spectrometer to determine the concentration of metal atoms in the nanocomposite. The Agilent Duo system consisting of 200 series AA and GTA 120 graphite tube atomizer controlled by one computer was used. The Agilent AA system software (SpectrAA) contained pre-set spectrometer parameters for iron and nickel and these were used to measure the samples. The morphology of the iron oxide/nickel oxide nanocomposite was determined by the scanning electron microscope

(Tescan Vega 3, SBU 118-0015, Brno, Czech Republic). The sample was fixed on a sample tab by carbon-double-sided adhesive carbon tape, vacuum dried, and scanned at an accelerating voltage of 5 kV. The adjustment knob was moved up and down until clear images were obtained and captured under secondary electron (SE) detectors. The Image J software was used to determine the area of the catalyst nanoparticles. The length of the nanoparticles was calculated in nanometers. The Originlab software was used to determine the size distribution of the nanoparticles.

Compounds in the bio-oil were dissolved in hexane and analyzed by a GC-MS analyzer (TQ8040 Shimadzu from UK). Chromatographic conditions were: HP-5 dimethylpolysiloxane column (30 m × 0.25 mm × 0.25 μm) with helium as the carrier gas and flow rate of 1.77 ml/min. The inlet temperature was 250 °C, the split ratio was 1.0, and the injection volume was 50 μl. Programmed heating: the initial temperature was 80 °C, maintained for 5 min, and then increased to 300 °C at a rate of 4 °C/min and maintained for an additional 7 min. MS conditions were as follows: Electron ionization (EI) source, ion source temperature of 230 °C, multiplier voltage of 300 V, interface temperature of 250 °C, and solvent delay time of 3.5 min. The NIST 98 spectrum library was used to compare the peaks for compound identification and the peak area for quantification.

2.2.6. Experimental Design by RSM

In the present work, a central composite design (CCD) was used to determine the effects of three independent variables (temperature, residence time, and catalyst dosage) on the yield of bio-oil and to study the interactions among the variables during the hydrothermal liquefaction of water hyacinth using iron oxide/nickel oxide nanocomposite. The input variables to be optimized were temperature (260 °C to 320 °C), residence time (15 minutes to 60 minutes), and catalyst concentration (0.25 g to 1.5 g). The output response was the bio-oil yield. For statistical analysis, variable levels were normalized to -1 (low), 0 (central), and 1 (high) according to the face-centered design ($\alpha = 1$). The software was used to create the experimental design. **Table 1** shows a design in absence of the catalysts containing 5 center points, and 8 non-center points, making a total of 13 runs. **Table 2** shows a design in presence of iron oxide/nickel oxide nanocomposite containing 8 cubic points, 6 hub points, and 1 center point repeated six times making a total of 20 runs. The bio-oil yield obtained in these experiments was optimized at various levels of parameters

3. Results and Discussion

3.1. Characterization of the Catalyst Nanoparticles

The crystalline nature and surface morphology of the iron oxide nanocatalyst was determined using X-ray diffraction and electron microscopy techniques (**Figure 2** and **Figure 3** respectively). The XRD spectrum of the iron oxide nanoparticles (**Figure 2**) revealed reflections that correspond to magnetite nanoparticles found at $2\theta = 30.437^\circ$, 35.715° , 43.393° , 53.950° , and 57.309° corresponding

Table 1. The central composite matrix and response for Design Expert (version 13) software in absence of the catalyst.

Standard order	Run	Reaction conditions		Response
		A: Temperature (°C)	B: Time (minutes)	Bio-oil yield (%)
13	1	290	37.5	28.4
4	2	320	60	50.7
11	3	290	37.5	28
3	4	260	60	26.8
2	5	320	15	23.6
12	6	290	37.5	28.4
8	7	290	60	39.5
5	8	260	37.5	18
6	9	320	37.5	31.6
9	10	290	37.5	27.8
1	11	260	15	14.1
7	12	290	15	19.4
10	13	290	37.5	28.6

Table 2. The central composite matrix and response for Design Expert (version 13) software for iron oxide/nickel oxide nanocomposite.

Standard order	Run	Reaction conditions			Response
		A: Temperature (°C)	B: Time (minutes)	C: Catalyst (g)	Bio-oil yield (%)
11	1	290	15	0.875	48.2
16	2	290	37.5	0.875	46.8
6	3	320	15	1.5	49.2
1	4	260	60	0.25	36.2
3	5	260	15	0.25	36.2
12	6	290	60	0.875	56.2
7	7	260	60	1.5	44.2
20	8	290	37.5	0.875	48.4
14	9	290	37.5	1.5	54.4
2	10	320	15	0.25	41.6
8	11	320	60	1.5	59.4
10	12	320	37.5	0.875	50.8
9	13	260	37.5	0.875	38.2
15	14	290	37.5	0.875	47.0
17	15	290	37.5	0.875	48.8

Continued

19	16	290	37.5	0.875	48.8
5	17	260	15	1.5	44.8
4	18	320	60	0.25	54.2
13	19	290	37.5	0.25	45.2
18	20	290	37.5	0.875	48.8

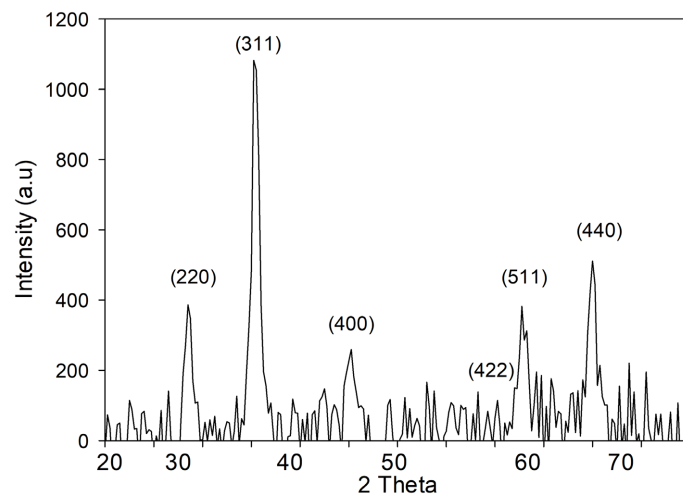


Figure 2. XRD spectrum of iron oxide nanocatalyst (magnetite).

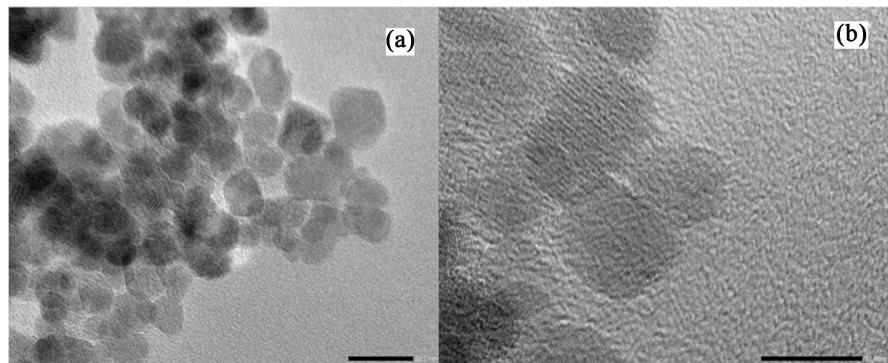


Figure 3. TEM images of iron oxide nanocatalyst (magnetite nanoparticles) showing the typical hexagonal shape of atoms 3a at a magnification of 20 nm and 3b at a magnification of 10 nm.

to the (220), (311), (400), (422), and (511) crystal planes of pure magnetite. These peaks match well with the reported peaks in the literature for magnetite [20]. **Figure 3** are TEM images showing the typical hexagonal structure of iron oxide nanocatalysts (magnetite nanoparticles). The nanoparticles were crystalline and monodispersed and had a size range between 10 - 12 nm. The particle size was determined using Image J software. The XRD spectrum and TEM images in **Figure 2** and **Figure 3** respectively confirm that iron oxide nanocatalysts were successfully synthesized.

In addition, SEM characterization (**Figure 4**) was performed to ascertain the

morphology and particle size of the iron oxide/nickel oxide nanocomposites. Image J software provided 463 particles in the image of iron oxide/nickel oxide nanocomposite. These results were fed into the Originlab software and the graph was plotted (Figure 5). The particle size distribution showed that the iron oxide/nickel oxide nanoparticles ranged from 10 nm to 60 nm.

From the histogram obtained from Originlab software, it was observed that the average particle size for iron oxide/nickel oxide nanocomposite was 27.5 nm.

The results obtained from the flame atomic absorption spectroscopy showed that the sample contained 34.2% iron and 63.4% nickel. The total percentage was less than 100%. This was due to the presence of oxygen in the samples since the catalyst nanoparticles synthesized were oxides and the technique doesn't detect non-metals.

3.2. Response Surface Models

The Design Expert software version 13 was used to analyze the experimental

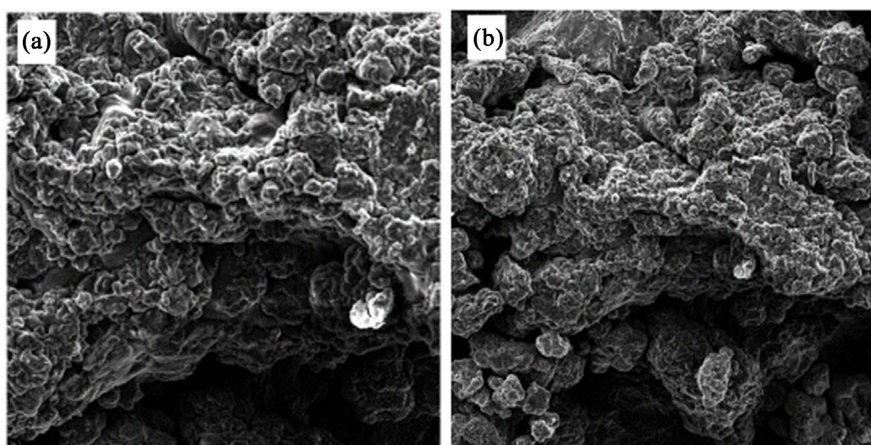


Figure 4. SEM images of iron oxide/nickel oxide nanocomposite synthesized by the co-precipitation method at a magnification of (a) 20 nm, (b) 50 nm.

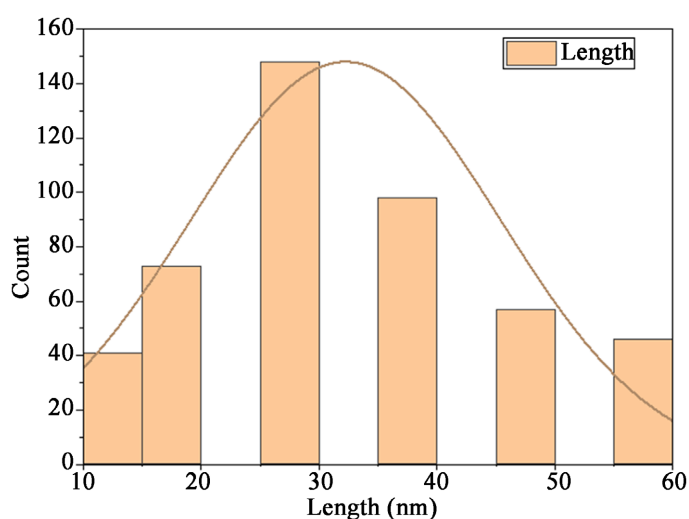


Figure 5. Particle size distribution of iron oxide/nickel oxide nanocomposite synthesized by co-precipitation method.

output results. The models were selected based on higher-order polynomials where the additional terms were significant and the models were not aliased. A quadratic model based on the coded values was found to best fit the responses. The significance of the model was evaluated based on a confidence interval of 95%. Equation (4) is the model equations for the prediction of bio-oil yield using iron oxide/nickel oxide nanocomposite.

$$Y_1 = 48.71 + 5.40A + 3.18B + 3.70C + 2.72AB - 0.275AC - 0.575BC - 5.18A^2 + 2.52B^2 + 0.1182C^2 \quad (4)$$

Y_1 is the bio-oil yield (wt%) obtained when iron oxide/nickel oxide nanocomposite was used as a catalyst, A is the temperature ($^{\circ}\text{C}$), B is the residence time (min), and C is the catalyst dosage (g). The analysis of variance (ANOVA) for the bio-oil yield using iron oxide/nickel oxide nanocomposite (**Table 3**) tested the statistical significance of the variables.

The sum of squares measured the deviation of data points away from the mean value. Df (degrees of freedom) indicated the number of independent values varied in analysis without violating the constraints. Mean squares were used to determine whether the terms in the model were significant. F-values were used to determine whether the test was statistically significant and the p-values indicated how compatible or incompatible the data were with a specified statistical model. The p-value of the models less than 0.05 indicated that the models were significant. The pure error of the models was also presented in the tables.

Table 3. ANOVA for the quadratic model for the bio-oil yield using iron oxide/nickel oxide nanocomposite.

Source	Sum of Squares	Df	Mean Square	F-value	p-value	Remarks
Model	678.13	9	75.35	40.60	<0.0001	Significant
A-Temperature	291.60	1	291.60	157.13	<0.0001	Significant
B-Time	101.12	1	101.12	54.49	<0.0001	Significant
C-Catalyst	136.90	1	136.90	73.77	<0.0001	Significant
AB	59.40	1	59.40	32.01	0.0002	Significant
AC	0.6050	1	0.6050	0.3260	0.5806	
BC	2.64	1	2.64	1.43	0.2601	
A ²	73.84	1	73.84	39.79	<0.0001	Significant
B ²	17.44	1	17.44	9.40	0.0119	Significant
C ²	0.0384	1	0.0384	0.0207	0.8885	
Residual	18.56	10	1.86			
Lack of Fit	14.34	5	2.87	3.40	0.1024	Not significant
Pure Error	4.21	5	0.8427			
Total	683.14	19				

Pure error mean square is the variance associated with error of replication indicating how well a design point can be repeated to obtain the same result.

The results demonstrated that terms A (temperature), B (Time), C (catalyst), AB, A², and B² had significant effects on the produced bio-oil yield (Y_1) whereas AC, BC, and C² had an insignificant impact on the bio-oil yield from the water hyacinth by hydrothermal liquefaction process using iron oxide/nickel oxide nanocomposite. The model F-value of 40.60 implies that the model is significant. There is only a 0.01% chance that an F-value this large could occur due to noise. The lack of fit F-value of 3.40 implies the Lack of Fit is not significant relative to the pure error. There is a 10.24% chance that a Lack of Fit F-value this large could occur due to noise. Non-significant lack of fit is good.

3.3. Effect of Process Conditions on Bio-Oil Yield

The RSM showed that temperature, catalyst, and residence time were all significant (**Table 3**). Increasing the temperature from 260°C to 320°C resulted in an increase in the bio-oil yield which could have been due to the extended biomass fragmentations with an increase in temperature [24]. Higher temperatures improve the cracking and the degradation reactions thus attaining maximum conversion of biomass to bio-oil [25]. The maximum bio-oil yield of 59.4 wt% (**Table 2**) was obtained at the temperature of about 320°C, 1.5 g of catalyst, and 60 minutes of residence time compared to 50.7 wt% (**Table 1**) in absence of the catalyst. At 260°C, 1.5 g of catalyst, and 60 minutes of residence time, a bio-oil yield of 44.2 wt% (**Table 2**) was obtained compared to 14.1 wt% (**Table 1**) obtained in the absence of the catalyst. This result revealed an improved biomass conversion rate at lower temperature reactions. This is because at higher temperature reactions the performance of the catalyst may reduce due to the enlargement of nanosized particles and reduction of the higher surface-volume ratio [26] [27].

The residence time had a slightly higher impact on bio-oil yield at high temperatures. This was attributed to the polymerization of small compounds to form bio-oil [5] [28]. At 320°C and 1.5 g of catalyst dosage, the yield increased by 10.2 wt% as the residence time increased from 15 minutes to 60 minutes. At lower temperatures of 260°C and 1.5 g of catalyst dosage, the bio-oil yield decreased by 0.6 wt% as the residence time increased from 15 minutes to 60 minutes. The conversion of bio-oil yield was more significant at low catalyst concentrations. In comparison with the previous study [5], iron oxide nanoparticles improved the conversion efficiency during the hydrothermal liquefaction of water hyacinth thus increase in the bio-oil yield. The bio-oil produced using iron oxide/nickel oxide nanocomposite was slightly higher than that produced when iron oxide nanocatalyst was used. This could be due to the exploitation of the synergistic effect of the two metal oxides and the opening up of the new catalytic avenues by the second metal oxide [29]. The optimal conditions were found to be a temperature of 282°C, 15 minutes, and 0.4 g of catalyst dosage which yielded 43.4 wt% bio-oil.

3.4. Optimization of Process Conditions Using Response Surface Plots

The impact of each factor on the yield of the bio-oil was demonstrated by the response surface and contour plots (Figures 6-8). The interaction effect of two factors in each plot was evaluated with one variable stable at zero level while the rest of the two factors were changed. These plots were used to observe how fitted responses were related to two continuous variables based on the model equations.

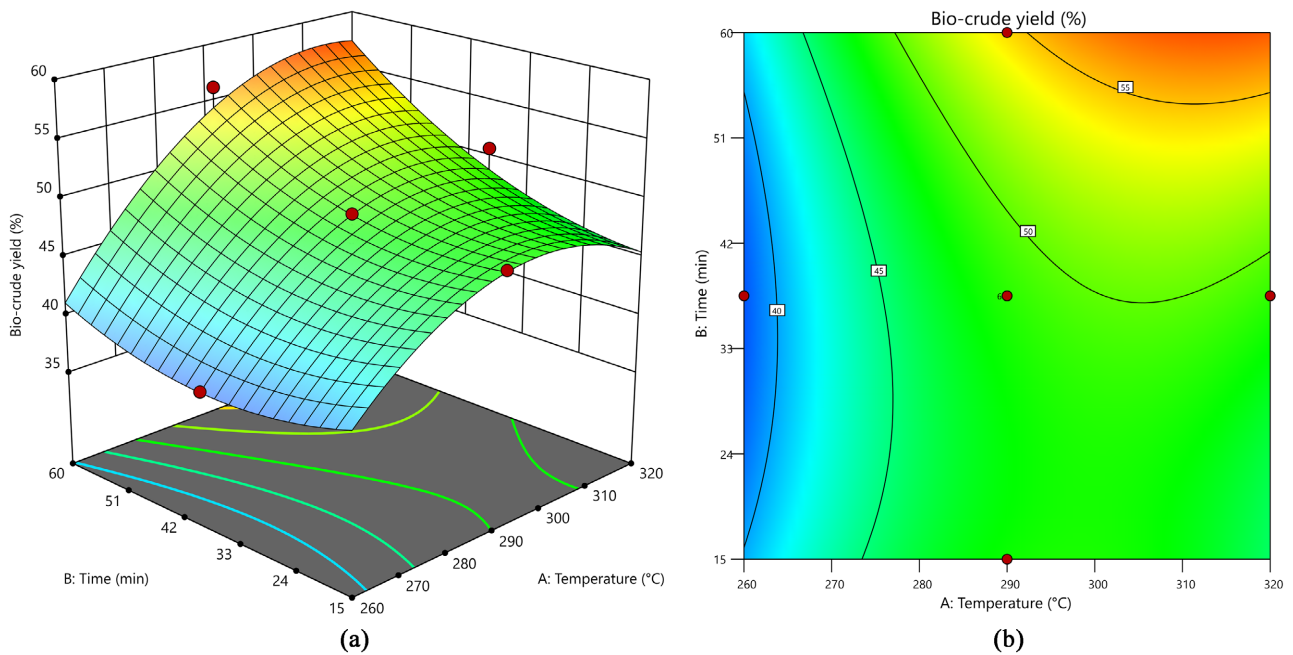


Figure 6. (a) Response surface and (b) contour plots of bio-oil yield as a function of temperature and residence time.

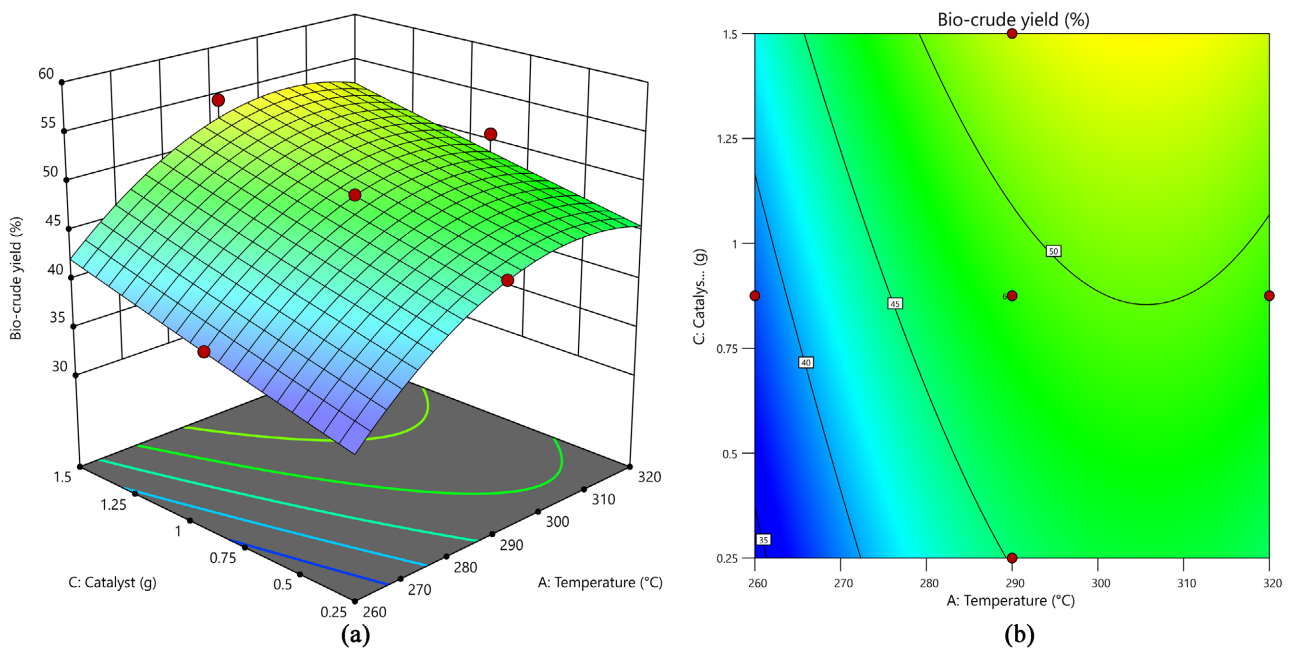


Figure 7. (a) Response surface and (b) contour plots of bio-oil yield as a function of temperature and catalyst.

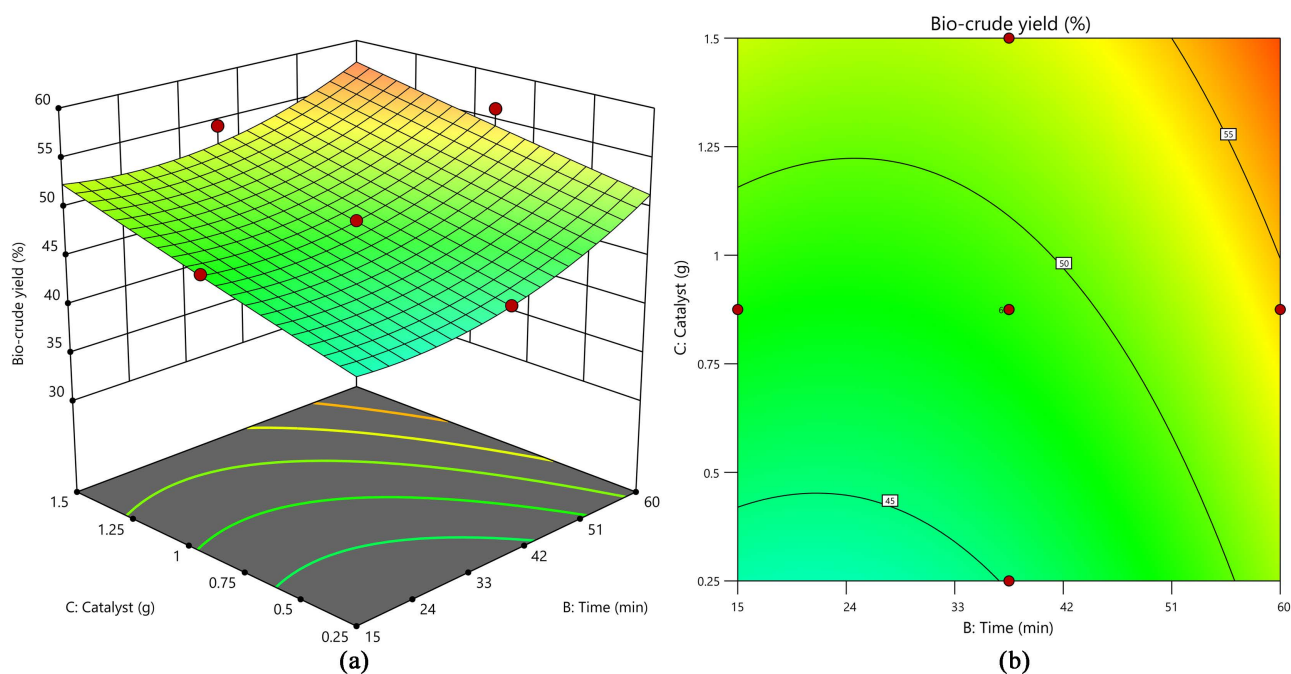


Figure 8. (a) Response surface and (b) contour plots of bio-oil yield as a function of residence time and catalyst.

The surface plots contain predictors on the x- and y-axes, and a continuous surface representing the fitted response values on the z-axis. The contour plots contain predictors on the x-axis and y-axis, contour lines that connect points that have the same fitted response values, and colored contour bands that represent ranges of the fitted response values (Figures 6-8). Surface plots and Contour plots were useful in establishing desirable response values and operating conditions using iron oxide/nickel oxide nanocomposite. The contour plot and response surface diagrams illustrated the effects of temperature vs. residence time (AB), temperature vs. catalyst (AC), and residence time vs. catalyst (BC). The impact of temperature and residence time on bio-oil yield is demonstrated in Figure 6(a) and Figure 6(b). From the response surface plot, the temperature played a crucial role in the hydrothermal liquefaction of water hyacinth. There was no significant bio-oil conversion obtained at higher temperatures and longer residence time. At 320 °C and 60 minutes of residence time, the bio-oil yield improved by 8.7 wt% using a catalyst (1.5 g) compared to the blank. In contrast, reducing the temperature with decreasing residence time, a significant conversion was obtained. The low temperature (260 °C), and shorter residence time (15 minutes) with catalyst dosage (1.5 g) provided an improvement of 30.7 wt% compared to the blank. The reduction in bio-oil yield at higher temperatures and longer residence times is attributed to the decomposition of the bio-oils into the gas phase in form of CO₂ [5]. These findings show that no significant conversion occurred in the higher temperature and longer residence time, and suggested the optimum bio-oil yield to be in lower temperatures and shorter residence time.

Figure 7(a) and Figure 7(b) shows the interactions of temperature and catalyst on bio-oil yield. The response surface plot demonstrates that the bio-oil

conversion is more significant at lower temperatures and lower catalyst concentrations. These plots also suggested that the temperature had a greater impact on the bio-oil yield which was attributed to the catalyst capability that could change the structure of biomass and help to emit the intracellular compounds such as carbohydrates and lipids and thus benefits the sequential liquefaction process towards bio-oil conversion [26] [30]. The bio-oil yield initially increased with increasing temperature up to 284°C and a further increase in temperature resulted in a decrease in bio-oil yield. This was attributed to the influence on the maximum depolymerization rate and hydrolyzation of biomass molecules by the increasing temperatures [31] while the reduction in bio-oil yield beyond the peak temperature was attributed to the Boudouard reactions [32]. **Figure 8(a)** and **Figure 8(b)** demonstrated the interaction between the residence time and the catalyst concentration. From the graphs, it was evidenced that the catalyst had a greater impact on bio-oil conversion compared to the residence time. At 260°C, 0.25 g of catalyst, and 60 minutes of residence time a bio-oil yield of 36.2 wt% was obtained. On decreasing the residence time to 15 minutes, the bio-oil yield increased to 37.8 wt%. This suggested that water hyacinth biomass can be converted to bio-oil in a shorter residence time and low catalyst dosage. Moreover, a high catalyst concentration leads to the deactivation of further depolymerization processes due to a reduction in catalytic reactivity [26] [33].

3.5. Catalyst Recovery and Re-Use for HTL

The catalyst recovery plays a crucial role in the hydrothermal liquefaction reaction for cost-effective measures of the process. After the hydrothermal liquefaction of water hyacinth, the nanoparticles were largely deposited in the solid residue. Magnetic separation was used to recover the nanoparticles. The recovered catalyst nanoparticles were reused and the bio-oil yields for fresh and recycled catalysts were compared in four cycles. All experiments were performed at 320°C, with 1.5 g for catalyst concentration for 60 minutes of residence time. After completing the first set of experiments, that same catalyst was recovered and reused for HTL reaction under the same conditions. In the first recycle, the iron oxide/nickel oxide showed a bio-oil yield of 57.1 wt% which was 2.3 wt% lesser than the fresh catalytic HTL reaction. Further, the catalysts were reused to four recycles, and the percentage of bio-oil yield production was illustrated in **Figure 9** below. There was a general decrease in bio-oil yield as the number of cycles increased. This was attributed to decreasing amount of recovered catalyst nanoparticles. In addition, the decrease is attributed to the morphological changes through particle size variation and increasing mass volume ratio [34] [35]. However, recycling the catalyst is very important because it can save on the cost of buying new catalysts for each batch hence making the process potentially economical.

3.6. GC-MS Analysis

The main chemical compounds were identified using GC-MS. The two bio-oil

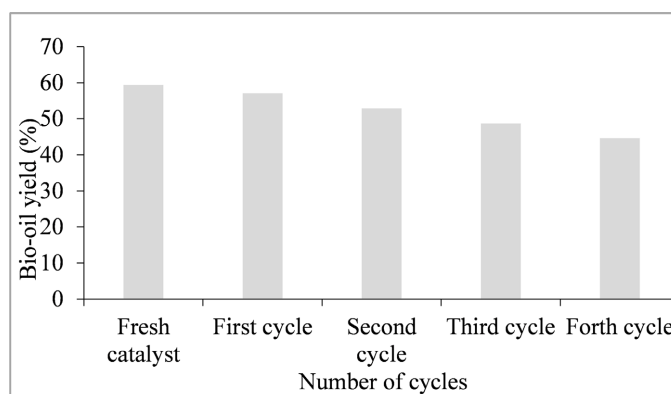


Figure 9. A comparison of bio-oil yields for the fresh and recycled catalyst in HTL of water hyacinth.

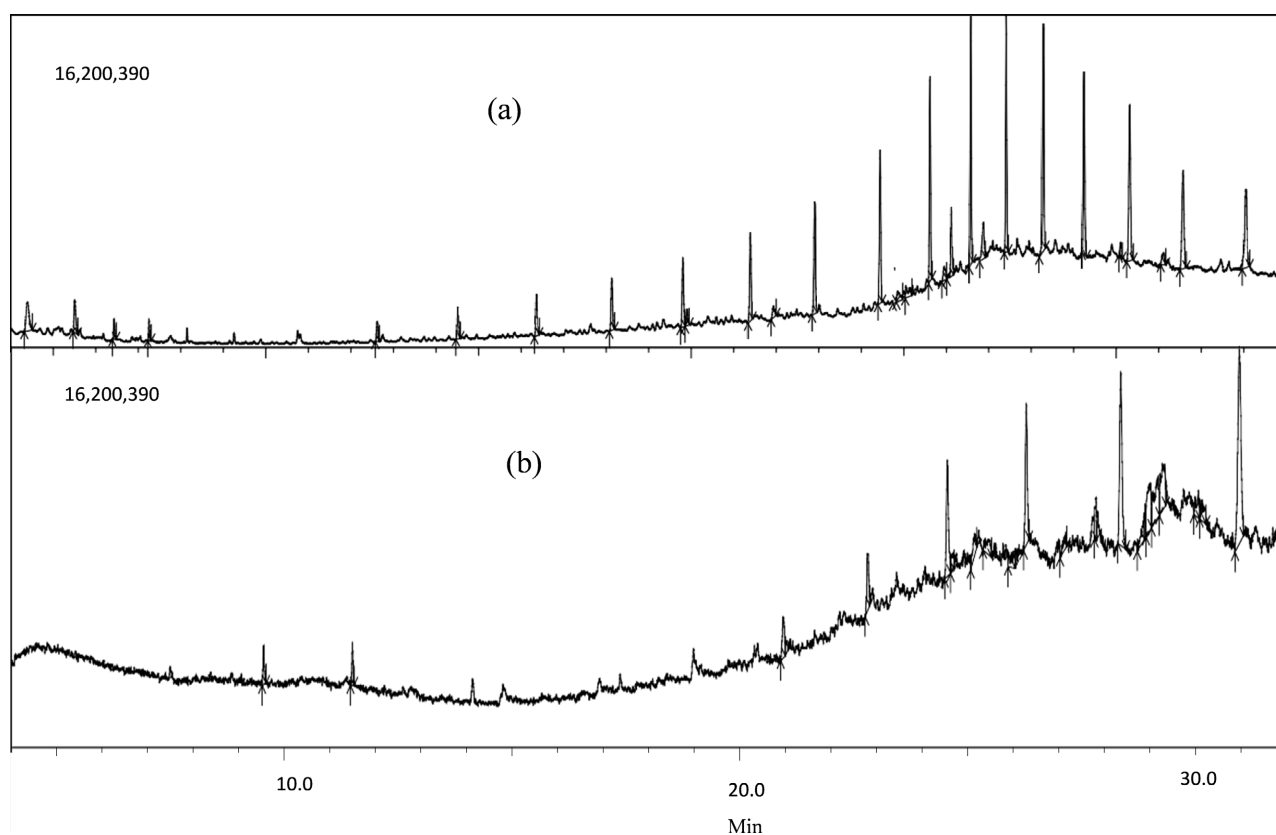


Figure 10. GC/MS of the water hyacinth bio-oil (a) in absence of catalyst (b) in presence of iron oxide/nickel oxide nanocomposite.

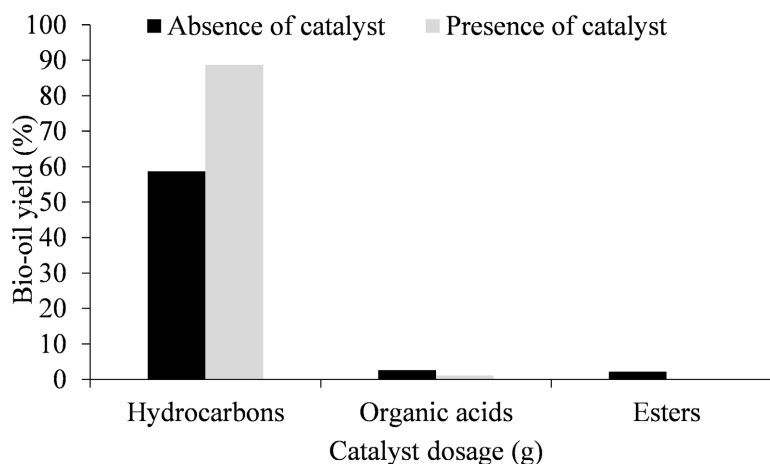
samples (blank and catalyst) were characterized by GC/MS. The NIST 98 spectrum library was used to identify the peaks. **Figure 10(a)** and **Figure 10(b)** shows the distribution of various bio-oil compounds in the presence and absence of the catalyst.

The peak area percentages of the major bio-oil compounds identified are shown in **Table 4**. Peaks in the GC-MS chromatogram with a percentage relative area of less than 1% were not considered.

The compounds obtained were grouped into hydrocarbons, organic acids, and esters as in **Figure 11**. The hydrocarbons identified included: undecane, dodecane,

Table 4. Table GC-MS major compounds in the absence and presence of a catalyst.

Retention time	Compounds	Relative area (%)		Chemical Formula
		Without catalyst	With catalyst	
4.39	Undecane	3.9	<1	C ₁₁ H ₂₄
5.501	Dodecane	3.5	<1	C ₁₂ H ₂₆
7.25	Tetradecane	1.0	<1	C ₁₄ H ₃₀
9.538	Hexadecane	<1	1.81	C ₁₆ H ₃₄
11.488	2-methyl tetracosane	<1	2.10	C ₂₅ H ₅₂
16.369	Nonadecane	6.4		C ₁₉ H ₄₀
18.806	Eicosane	9.2		C ₂₀ H ₄₂
19.905	Octadecyl acetate	1.2		C ₂₀ H ₄₀ O ₂
20.88	Heptadecane 2,6,10,15-tetramethyl		4.63	C ₂₁ H ₄₄
22.744	Pentacosane		11.89	C ₂₅ H ₅₂
24.785	Bis(2-ethylhexyl) phthalate	2.2		C ₂₄ H ₃₈ O ₄
24.85	Octadecyl acetate, eicosyl vinyl ester	1.4	1.1	C ₂₃ H ₄₄ O ₃
26.277	2-methyl hexacosane	1.83	9.09	C ₂₇ H ₅₆
28.282	Hexacosane	13.8	13.68	C ₂₆ H ₅₄
28.560	Hopane	2.4	2.6	C ₃₀ H ₅₂
29.005	Eicosane		19.73	C ₂₀ H ₄₂
30.952	Octacosane 2-methyl	7.80	23.13	C ₂₉ H ₆₀
33.048	Tetratriacontane	8.80		C ₃₄ H ₇₀
Total		63.43	89.76	

**Figure 11.** GC Distribution of major bio-oil compounds in the absence and presence of catalyst.

tetradecane, hexadecane, 2-methyl tetracosane, nonadecane, eicosane, heptadecane 2,6,10,15-tetramethyl, octacosane, 2-methyl, pentacosane, 2-methylhexacosane, hexacosane, hopane, and tetratriacontane. The organic acid grouping consisted of octadecyl acetate while the ester grouping consisted of Bis (2-ethylhexyl) phthalate.

The hydrocarbon grouping was the most dominant among the compounds obtained. During the uncatalyzed HTL, hexacosane registered the highest composition of 13.8% followed by eicosane (9.2%) and then octacosane 2-methyl (7.8%). When iron oxide/nickel oxide nanocomposite was used in the catalytic HTL of water hyacinth, octacosane 2-methyl, eicosane, hexacosane, and pentacosane had significantly high compositions of 23.13%, 19.73%, 13.68%, and 11.89%. The yield of Pentacosane increased greatly during catalytic hydrothermal liquefaction. During uncatalyzed HTL it was below 1% and increased to 11.89% using the iron oxide/nickel oxide nanocomposite. This revealed that catalyst nanocomposite could have played a catalytic role by favoring reactions that led to the decomposition of cellular components like carbohydrates and oils to produce more Pentacosane hence increasing the number of hydrocarbons in the bio-oils [5].

It is worth noting that the presence of catalyst produced bio-oil with a high hydrocarbon content, a low composition of oxygenated compounds (acids and esters), and a very low composition of nitrogenated, and Sulphur compounds to below detectable levels (below 1%) during the hydrothermal liquefaction of water hyacinth. In addition, the catalytic hydrothermal liquefaction demonstrated a significant decrease in the oxygenated compounds for example esters reduced to undetectable levels (below 1%). This shows that during the catalytic hydrothermal liquefaction, some of the oxygenated compounds may have been converted to hydrocarbons through decarboxylation reactions or other reaction pathways thus improving the bio-oil [5].

3.7. Elemental Analysis of Bio-Oil

The C, H, N, O, and S elemental analysis of bio-oil obtained at 320°C, for 60 minutes in the absence and presence of 1.5 g of the catalyst was done and the results were recorded (Table 5). The choice of these parameters was based on the fact that they led to the production of the highest bio-oil yield in the presence and absence of the catalyst. The aim was to determine the effect of the different catalysts on the bio-oil composition, High heating value (HHV), and energy recovery (ER). The water hyacinth biomass had an ash content of 16.9% and a moisture content of 8%. When hydrothermal liquefaction of water hyacinth was performed, the bio-oil which was produced in presence of the catalysts had higher yields of carbon, and hydrogen contents compared to the bio-oil produced in absence of the catalysts (Table 5). The carbon content (35.1 wt%) of the biomass increased to 68.6 wt% when the biomass was subjected to a hydrothermal liquefaction process without a catalyst. On performing catalytic hydrothermal

Table 5. Elemental composition, HHV, and ER of biomass and bio-oil produced at 320°C, for 60 minutes from HTL of water hyacinth biomass in the absence and presence of 1.5 g catalyst nanoparticles.

Content	Elemental composition (wt%)		
	Biomass [5]	Without a catalyst [5]	With catalyst
C (wt%)	35.1 ± 0.06	68.6 ± 0.12	74.4 ± 0.03
H (wt%)	6.10	8.10 ± 0.06	9.80 ± 0.04
N (wt%)	5.40 ± 0.06	2.80 ± 0.03	1.80 ± 0.01
O (wt%)	52.1 ± 0.01	7.40 ± 0.14	2.90 ± 0.21
S (wt%)	0.60 ± 0.01	0.45	0.23 ± 0.01
N/C*	0.11	0.03	0.02
H/C*	2.09	1.42	1.57
O/C*	6.41	0.69	0.03
HHV (MJ/Kg)	11.3 ± 0.2	33.5 ± 0.16	38.6 ± 0.01
ER (%)	0.0	62.6 ± 0.06	81.5 ± 0.07

*Atomic ratios.

liquefaction, the bio-oil produced using iron oxide/nickel oxide nanocomposite presented a higher carbon content of 74.4 wt%. These results showed that the hydrothermal liquefaction led to an increase in the hydrogen and carbon content of the bio-oil compared to the biomass from which it was derived. It was also evidenced that the presence of a catalyst favored the reactions responsible for increasing the carbon and hydrogen contents in the bio-oil. This could be due to the presence of Fe₃O₄ which is recognized to have a catalytic effect in hydrogenation reactions [14]. This trend was also observed in the study of [5] [14] [31] [34].

The nitrogen, oxygen, and Sulphur content in the bio-oil was lower than that in the water hyacinth biomass from which it was derived. The bio-oil produced from the catalyzed hydrothermal liquefaction had lower N, O, and S content compared to that from the uncatalyzed hydrothermal liquefaction. The nitrogen content in the biomass feedstock (5.4 wt%) decreased to 2.8 wt% after subjecting the biomass to hydrothermal liquefaction without a catalyst. The nitrogen content was further reduced to 1.8 wt% using iron oxide/nickel oxide nanocomposite in the hydrothermal liquefaction which is essential in improving the high heating value of the bio-oil and reducing the release of harmful noxious gases (NO_x) into the atmosphere. This was also observed in studies conducted by [5] [31].

The oxygen composition reduced from 52.1 wt% in the biomass feedstock to 7.4 wt% in bio-oil produced from uncatalyzed hydrothermal liquefaction of water hyacinth. The introduction of iron oxide/nickel oxide further reduced the oxygen content in the bio-oil to 2.9 wt%. This was evident that the synergistic

effect of nickel oxide led to the superior catalytic activity of the iron oxide nanocatalyst for the deoxygenation of bio-oil. A similar trend was observed in the studies conducted by [31] [34] [36]. Deoxygenation is potentially achieved through the loss of oxygen into the gas phase in form of CO and CO₂ [5]. Removal of oxygen from bio-oil increases its high heating value and energy recovery making it potentially competitive with petroleum-derived fuels.

The Sulphur composition was reduced from 0.6 wt% in biomass feedstock to 0.41 wt% when the biomass underwent hydrothermal liquefaction in the absence of the catalyst. The Sulphur content was further reduced to 0.23 wt% when the bio-oil was produced from catalyzed hydrothermal liquefaction using iron oxide/nickel oxide nanocomposite. High Sulphur content in bio-oil is responsible for the production of dangerous gases such as Sulphur dioxide gas thus the formation of acid rains. The presence of high hetero atom content in the bio-oil imparts undesirable fuel characteristics such as high viscosity and acidity leading to a negative effect on storage stability, combustion performance, and economic value [37] [38] [39]. These results suggested that the catalysts facilitated desulphurization, deoxygenation, and denitrogenation reactions during the hydrothermal liquefaction of water hyacinth thus improving the quality of the bio-oil produced.

The HHV which indicates the upper limit of the available thermal energy produced by the complete combustion of fuel was used to evaluate the energy performance of the bio-oil produced. The HHV of biomass (11.3 MJ/Kg) increased to 33.5 MJ/Kg for the uncatalyzed hydrothermal liquefaction. The bio-oil produced during the catalytic hydrothermal liquefaction presented an HHV of 38.6 MJ/Kg when the iron oxide was modified with nickel oxide to form a nanocomposite. These results demonstrated that the catalyzed hydrothermal liquefaction led to a higher HHV than uncatalyzed hydrothermal liquefaction thus better quality and improved energy performance of the bio-oil. This is because, during the catalyzed hydrothermal liquefaction, a higher C and H content of bio-oil was achieved leading to higher HHV. Modifying iron oxide with nickel oxide improved the HHV of the bio-oil produced from water hyacinth compared to the previous studies on the hydrothermal liquefaction of water hyacinth [5] [8]. Furthermore, the low heteroatom contents in bio-oil from catalyzed HTL contributed to the increase in the HHV. This combined effect led to bio-oil produced from catalyzed hydrothermal liquefaction having a higher HHV than bio-oil produced from uncatalyzed hydrothermal liquefaction. A similar trend was observed in the study conducted by [34] where they attributed it to the decarboxylation mechanism during the production of bio-oil from hydrothermal liquefaction of *Spirulina platensis* using Fe₃O₄ catalyzed.

The energy recovery in the current study increased from 62.6% to 81.4 wt% when the water hyacinth was subjected to hydrothermal liquefaction in the absence of a catalyst and the presence of iron oxide/nickel oxide nanocomposite respectively. This demonstrates that a modified iron oxide nanocatalyst with nickel

oxide in the production of bio-oil from hydrothermal liquefaction of water hyacinth could be an efficient and economically favorable method.

The O/C, H/C, and N/C atomic ratios were also calculated. The O/C ratio of the biomass (6.41) was reduced to 0.69 during the uncatalyzed hydrothermal liquefaction. The ratio further decreased to 0.03 wt% when iron oxide/nickel oxide nanocomposite was used. The O/C ratio indicated the polarity and abundance of polar oxygen-containing surface functional groups in the bio-oil. A higher O/C ratio indicated that there were more polar functional groups in the oil and a lower O/C ratio indicated that there were fewer polar functional groups in the oil or a reduction in the polarity of the oil [5].

The biomass had an H/C ratio of 2.09 which was reduced to 1.42 during the uncatalyzed hydrothermal liquefaction. When the iron oxide was modified with nickel oxide, the H/C ratio increased to 1.57. The H/C ratio indicates the aromaticity of the fuel, the higher the H/C ratio, the higher the energy efficiency of the bio-oil and the lower the CO₂ emissions from its combustion. The lower the H/C ratio, the lower the energy efficiency of the fuel and the higher the CO₂ emissions since it is very difficult to burn the fuel without the production of carbon [39]. From these results, it is evident that modifying iron oxide with nickel oxide improved the energy efficiency of the bio-oil.

The N/C ratio reduced steadily from 0.11 in the biomass feedstock to 0.03 in uncatalyzed bio-oil and 0.02 when iron oxide/nickel oxide nanocomposite was used in the hydrothermal liquefaction of water hyacinth. A high N content in the fuel is undesirable since it leads to the production of NO_x gases during combustion. The results showed that catalytic hydrothermal liquefaction increased the removal of N compounds from the bio-oil hence reduction in the N/C ratio.

4. Conclusions

The iron oxide nanocatalyst and iron oxide/nickel oxide nanocomposite were synthesized using the co-precipitation method and characterized using XRD, TEM, SEM, and AAS. The nickel content of 63.4% and iron content of 34.2% was obtained in iron oxide/nickel oxide nanocomposite. TEM results showed that iron oxide nanocatalysts had particle sizes ranging from 10 - 12 nm and when modified with nickel oxide, the average particle size of 27.5 nm was obtained from SEM results.

Hydrothermal liquefaction process conditions were optimized using a central composite design of response surface methodology to enhance the process economy by increasing the yield at low temperatures, less residence time, and minimum catalyst dosage. The optimum conditions obtained were 282°C, 15 minutes, and 0.4 g of catalyst yielding 43.4 wt% of bio-oil.

The catalysts were easily recovered by magnetic separation and reused four times without significant loss in performance. The recycled iron oxide/nickel oxide nanocomposite produced a bio-oil yield of 57.1 wt% during the first cycle to 44.6 wt% in the fourth cycle.

The bio-oil produced was characterized using GC-MS and CHNSO elemental analysis. When iron oxide/nickel oxide nanocomposite was used in hydrothermal liquefaction of water hyacinth, GC-MS results revealed that the percentage composition of hydrocarbons in the bio-oil increased by 30.03 wt%, respectively compared to the uncatalyzed hydrothermal liquefaction. In addition, further gains in hydrocarbon yields and improvement of the quality of bio-oil could be achieved when HTL is done in presence of suitable catalysts. Moreover, modifying iron oxide with nickel oxide greatly improved the catalytic activity of the iron oxide nanocatalyst especially, in the deoxygenation of bio-oil.

The preliminary characterization of bio-oil exhibited a higher energy performance compared to previous studies on the hydrothermal liquefaction of water hyacinth. This was observed from the elemental composition analysis results which showed that the carbon content in the bio-oil increased by 5.8 wt% when catalyzed by iron oxide/nickel oxide nanocomposite. A similar trend was observed in the results of hydrogen content in bio-oil produced. The percentage of hetero atom compounds, nitrogen, and oxygen in the bio-oil reduced when HTL was done in the presence of a catalyst hence increasing the HHV of the bio-oil produced. This revealed that the nanocomposites used had a great catalytic activity in increasing the yield and quality of the bio-oil from the hydrothermal liquefaction of water hyacinth.

Acknowledgments

This work was funded by the Government of the Republic of Uganda through the Makerere University Research and Innovations Fund (Grant number: MAK RIF/CONAS/004).

Conflicts of Interest

The authors declare no conflicts of interest regarding the publication of this paper.

References

- [1] Muhammad, U.L., Shamsuddin, I.M., Danjuma, A., Musawa, S. and Dembo, U.H. (2019) Biofuels as the Starring Substitute to Fossil Fuels Biofuels as the Starring Substitute to Fossil Fuels. *Petroleum Science and Engineering*, **2**, 44-49. <https://doi.org/10.11648/j.pse.20180201.17>
- [2] Galadima, A. and Muraza, O. (2017) Hydrothermal Liquefaction of Algae and Bio-Oil Upgrading into Liquid Fuels: Role of Heterogeneous Catalysts. *Renewable and Sustainable Energy Reviews*, **81**, 1037-1048. <https://doi.org/10.1016/j.rser.2017.07.034>
- [3] Patel, B., Tamburic, B., Zemichael, F.W., Dechatiwongse, P. and Hellgardt, K. (2012) Algal Biofuels: A Credible Prospective? *International Scholarly Research Notices*, **2012**, Article ID: 631574. <https://doi.org/10.5402/2012/631574>
- [4] Azadi, P., Afif, E., Foroughi, H., Dai, T., Azadi, F. and Farnood, R. (2013) Catalytic Reforming of Activated Sludge Model Compounds in Supercritical Water Using Nickel and Ruthenium Catalysts. *Applied Catalysis B: Environmental*, **134-135**,

- 265-273. <https://doi.org/10.1016/j.apcatb.2013.01.022>
- [5] Egesa, D., Mulindwa, P., Mubiru, E., Kyomuhimbo, H.D. and Aturagaba, G. (2021) Hydrothermal Liquefaction of Water Hyacinth : Effect of Process Conditions and Magnetite Nanoparticles on Biocrude Yield and Composition. *Journal of Sustainable Bioenergy Systems*, **11**, 157-186. <https://doi.org/10.4236/jsbs.2021.114012>
- [6] Duan, P. and Savage, P.E. (2011) Catalytic Hydrotreatment of Crude Algal Bio-Oil in Supercritical Water. *Applied Catalysis B: Environmental*, **104**, 136-143. <https://doi.org/10.1016/j.apcatb.2011.02.020>
- [7] Nanda, S., Rana, R., Sarangi, P.K., Dalai, A.K. and Kozinski, J.A. (2018) A Broad Introduction to First-, Second-, and Third-Generation Biofuels. In: Sarangi, P., Nanda, S. and Mohanty, P., Eds., *Recent Advancements in Biofuels and Bioenergy Utilization*, Springer, Singapore, 1-25.
- [8] Nallasivam, J. and Eboibi, B.E. (2020) Hydrothermal Liquefaction of Water Hyacinth (*Eichhornia crassipes*): Influence of Reaction Temperature on Product Yield, Carbon and Energy Recovery, and Hydrocarbon Species Distribution in Biocrude. *Biomass Conversion and Biorefinery*, **12**, 3827-3841. <https://doi.org/10.1007/s13399-020-01032-1>
- [9] Phothisantikul, P.P., Tuanpusa, R., Nakashima, M., Charinpanitkul, T. and Matsu-mura, Y. (2013) Effect of CH₃COOH and K₂CO₃ on Hydrothermal Pretreatment of Water Hyacinth (*Eichhornia crassipes*). *Industrial & Engineering Chemistry Research*, **52**, 5009-5015. <https://doi.org/10.1021/ie302434w>
- [10] Bergier, I., Salis, S.M., Miranda, C. and Ortega, E. (2012) Biofuel Production from Water Hyacinth in the Pantanal Wetland. *Ecohydrology & Hydrobiology*, **12**, 77-84. <https://doi.org/10.2478/v10104-011-0041-4>
- [11] Gollakota, A.R.K., Kishore, N. and Gu, S. (2018) A Review on Hydrothermal Liquefaction of Biomass. *Renewable and Sustainable Energy Reviews*, **81**, 1378-1392. <https://doi.org/10.1016/j.rser.2017.05.178>
- [12] Egesa, D., Plucinski, P. and Chuck, C.J. (2023) Catalytic Hydrothermal Liquefaction of Magnetically Separated Microalgae : Effect of Reaction Conditions on Bio-Crude Yield and Composition. *Biomass Conversion and Biorefinery*.
- [13] Castello, D. and Pedersen, T.H. (2018) Continuous Hydrothermal Liquefaction of Biomass : A Critical Review. *Energies*, **11**, Article 3165. <https://doi.org/10.3390/en11113165>
- [14] de Caprariis, B., Bavasso, I., Bracciale, M.P., Damizia, M., De Filippis, P. and Scarsella, M. (2018) Enhanced Bio-Crude Yield and Quality by Reductive Hydrothermal Liquefaction of Oak Wood Biomass: Effect of Iron Addition. *Journal of Analytical and Applied Pyrolysis*, **139**, 123-130. <https://doi.org/10.1016/j.jaap.2019.01.017>
- [15] Nagappan, S., Bhosale, R.R., Duc, D., Thuy, N. and Chi, L. (2021) Catalytic Hydrothermal Liquefaction of Biomass into Bio-Oils and Other Value-Added Products—A Review. *Fuel*, **285**, Article ID: 119053. <https://doi.org/10.1016/j.fuel.2020.119053>
- [16] Tian, C., Li, B., Liu, Z., Zhang, Y. and Lu, H. (2014) Hydrothermal Liquefaction for Algal Biorefinery : A Critical Review. *Renewable and Sustainable Energy Reviews*, **38**, 933-950. <https://doi.org/10.1016/j.rser.2014.07.030>
- [17] Xu, D., Lin, G., Guo, S., Wang, S., Guo, Y. and Jing, Z. (2018) Catalytic Hydrothermal Liquefaction of Algae and Upgrading of Biocrude : A Critical Review. *Renewable and Sustainable Energy Reviews*, **97**, 103-118. <https://doi.org/10.1016/j.rser.2018.08.042>

- [18] Yadav, P. and Reddy, S.N. (2020) Bioresource Technology Hydrothermal Liquefaction of Fe-Impregnated Water Hyacinth for Generation of Liquid Bio-Fuels and Nano Fe Carbon Hybrids. *Bioresource Technology*, **313**, Article ID: 123691. <https://doi.org/10.1016/j.biortech.2020.123691>
- [19] Singh, R., Balagurumurthy, B. and Prakash, A. (2014) Catalytic Hydrothermal Liquefaction of Water Hyacinth. *Bioresource Technology*, **178**, 157-165. <https://doi.org/10.1016/j.biortech.2014.08.119>
- [20] Egesa, D., Chuck, C.J. and Plucinski, P.K. (2017) Multifunctional Role of Magnetic Nanoparticles in Efficient Microalgae Separation and Catalytic Hydrothermal Liquefaction. *ACS Sustainable Chemistry & Engineering*, **6**, 991-999. <https://doi.org/10.1021/acssuschemeng.7b03328>
- [21] Choo, M.Y., et al. (2020) Deoxygenation of Triolein to Green Diesel in the H₂-Free Condition: Effect of Transition Metal Oxide Supported on Zeolite Y. *Journal of Analytical and Applied Pyrolysis*, **147**, Article ID: 104797. <https://doi.org/10.1016/j.jaap.2020.104797>
- [22] Mahmaoodi, E. and Behnajady, M.A. (2018) Synthesis of Fe₃O₄@NiO Core-Shell Nanocomposite by the Precipitation Method and Investigation of Cr(VI) Adsorption Efficiency. *Colloids and Surfaces A: Physicochemical and Engineering Aspects*, **538**, 287-296. <https://doi.org/10.1016/j.colsurfa.2017.11.020>
- [23] Smith-Baedorf, H., et al. (2016) Assessing Hydrothermal Liquefaction for the Production of Bio-Oil and Enhanced Metal Recovery from Microalgae Cultivated on Acid Mine Drainage. *Fuel Processing Technology*, **142**, 219-227. <https://doi.org/10.1016/j.fuproc.2015.10.017>
- [24] Akhtar, J., Aishah, N. and Amin, S. (2011) A Review on Process Conditions for Optimum Bio-Oil Yield in Hydrothermal Liquefaction of Biomass. *Renewable and Sustainable Energy Reviews*, **15**, 1615-1624. <https://doi.org/10.1016/j.rser.2010.11.054>
- [25] Valle, B., Aramburu, B., Olazar, M., Bilbao, J. and Gayubo, A.G. (2017) Steam Reforming of Raw Bio-Oil over Ni/La₂O₃- α Al₂O₃: Influence of Temperature on Product Yields and Catalyst Deactivation. *Fuel*, **216**, 463-474. <https://doi.org/10.1016/j.fuel.2017.11.149>
- [26] Kandasamy, S., et al. (2019) Effect of Low-Temperature Catalytic Hydrothermal Liquefaction of *Spirulina platensis*. *Energy*, **190**, Article ID: 116236. <https://doi.org/10.1016/j.energy.2019.116236>
- [27] Yan, C.F., Cheng, F.F. and Hu, R.R. (2010) Hydrogen Production from Catalytic Steam Reforming of Bio-Oil Aqueous Fraction over Ni/CeO₂-ZrO₂ Catalysts. *International Journal of Hydrogen Energy*, **35**, 11693-11699. <https://doi.org/10.1016/j.ijhydene.2010.08.083>
- [28] Biller, P. and Ross, A.B. (2011) Bioresource Technology Potential Yields and Properties of Oil from the Hydrothermal Liquefaction of Microalgae with Different Biochemical Content. *Bioresource Technology*, **102**, 215-225. <https://doi.org/10.1016/j.biortech.2010.06.028>
- [29] Reuben Hudson, A.M. and Feng, Y.T. (2014) Bare Magnetic Nanoparticles: Sustainable Synthesis and Applications in Catalytic Organic Transformations. *Green Chemistry*, **16**, 4493-4505. <https://doi.org/10.1002/chin.201450226>
- [30] Demiral, I. (2008) Bioresource Technology the Effects of Different Catalysts on the Pyrolysis of Industrial Wastes (Olive and Hazelnut Bagasse). *Bioresource Technology*, **99**, 8002-8007. <https://doi.org/10.1016/j.biortech.2008.03.053>
- [31] Cao, M., Long, C., Sun, S., Zhao, Y., Luo, J. and Wu, D. (2021) Catalytic Hydro-

- thermal Liquefaction of Peanut Shell for the Production Aromatic Rich Monomer Compounds. *Journal of the Energy Institute*, **96**, 90-96. <https://doi.org/10.1016/j.joei.2021.02.007>
- [32] Toor, S.S., Rosendahl, L. and Rudolf, A. (2011) Hydrothermal Liquefaction of Biomass: A Review of Subcritical Water Technologies. *Energy*, **36**, 2328-2342. <https://doi.org/10.1016/j.energy.2011.03.013>
- [33] Tian, W., Liu, R., Wang, W., Yin, Z. and Yi, X. (2018) Effect of Operating Conditions on Hydrothermal Liquefaction of *Spirulina* over Ni/TiO₂ Catalyst. *Bioresource Technology*, **263**, 569-575. <https://doi.org/10.1016/j.biortech.2018.05.014>
- [34] Kandasamy, S., *et al.* (2019) Biomass and Bioenergy Hydrothermal liquefaction of Microalgae Using Fe₃O₄ Nanostructures as Efficient Catalyst for the Production of Bio-Oil: Optimization of Reaction Parameters by Response Surface Methodology. *Biomass and Bioenergy*, **131**, Article ID: 105417. <https://doi.org/10.1016/j.biombioe.2019.105417>
- [35] Raikova, S., Le, C.D., Beacham, T.A., Jenkins, R.W., Allen, M.J. and Chuck, C.J. (2017) Biomass and Bioenergy towards a Marine Biorefinery through the Hydrothermal Liquefaction of Macroalgae Native to the United Kingdom. *Biomass and Bioenergy*, **107**, 244-253. <https://doi.org/10.1016/j.biombioe.2017.10.010>
- [36] Zhou, D., Zhang, L., Zhang, S., Fu, H. and Chen, J. (2010) Hydrothermal Liquefaction of Macroalgae *Enteromorpha prolifera* to Bio-Oil. *Energy & Fuels*, **24**, 4054-4061. <https://doi.org/10.1021/ef100151h>
- [37] Hariani, P.L., Faizal, M. and Setiabudidaya, D. (2013) Synthesis and Properties of Fe₃O₄ Nanoparticles by Co-Precipitation Method to Removal Procion Dye. *International Journal of Environmental Science and Development*, **4**, 336-340. <https://doi.org/10.7763/IJESD.2013.V4.366>
- [38] Huber, G.W., Iborra, S. and Corma, A. (2006) Synthesis of Transportation Fuels from Biomass: Chemistry, Catalysts, and Engineering. *Chemical Reviews*, **106**, 4044-4098. <https://doi.org/10.1021/cr068360d>
- [39] Rafiq, M.K., Bachmann, R.T., Rafiq, M.T., Shang, Z., Joseph, S. and Long, R. (2016) Influence of Pyrolysis Temperature on Physico-Chemical Properties of Corn Stover (*Zea mays* L.) Biochar and Feasibility for Carbon Capture and Energy Balance. *PLOS ONE*, **11**, e0156894. <https://doi.org/10.1371/journal.pone.0156894>